A Proposed Entry Vehicle Dynamic Model

A. A. KIRSCH*
General Electric Company, King of Prussia, Pa.

A theory is proposed in this paper which provides an explanation and a mechanism for the dynamic stability problem of re-entry vehicles. The approach is based on the random fluctuating surface pressures present in the boundary layer when boundary-layer transition moves on to the vehicle aft end. These fluctuating pressures, when integrated circumferentially, produce a net fluctuating lateral load and therefore a fluctuating moment about the vehicle c.g. which can tune with the fundamental re-entry vehicle pitch frequency and feed energy into the system. The vehicle then becomes unstable and diverges. It will be shown that with this formulation there now exists a mechanism which can make flight vehicles enter the divergence region, as well as, exit; a requirement not fulfilled by any of the theories proposed to date, except hypothetically. In addition, the magnitude of the angle-of-attack divergence can potentially be predicted prior to flight with this technique. The present analytical model was applied to flight vehicles having no unusual configuration characteristics which could drastically perturb the local flow conditions. The results indicate extremely good correlation with flight data whether the vehicles are sharp or blunt, small or large, and for all types of heat shields.

Nomenclature

A_α	= aerodynamic restoring moment, ft-lb
$B_{\dot\alpha}$	= aerodynamic damping moment, ft-lb-sec
C_1, C_2	= coefficients
C_D	= drag coefficient
$C_{m\alpha}$	= static stability derivative, 1/rad
$C_{mq} + C_{m\dot\alpha}$	= dynamic stability derivative, 1/rad
$C_{N\alpha}$	= normal force coefficient slope, 1/rad
D_{REF}	= reference length, ft
$f(X_{CG}, X_o, \Theta_c)$	= function defined in Eq. (A.15)
I	= vehicle mass moment of inertia, slug-ft^2
L	= vehicle length measured from apex, ft
M	= vehicle mass, slugs
$M(t)$	= time dependent pitching moment, ft-lbs
$\dot m$	= mass addition rate ($\dot m/\rho_\infty U_\infty S_{REF}$)
$\bar p_{RMS}$	= root-mean-square fluctuating, psf, pressures based on boundary-layer edge properties
$\Delta p(X, \Theta, t)$	= random fluctuating surface pressure, psf
q_∞	= freestream dynamic pressure, psf
Q_{α^2}	= power spectral density of the pitching moment, ft-lb/rad/sec
R	= local vehicle radius, ft
S_{REF}	= reference area, ft^2
U_∞	= freestream velocity, fps
U_c	= convection velocity, fps, ($U_c = 0.6$ to $0.8\ U_e$)
U_e	= boundary-layer edge velocity, fps
X_{CG}	= c.g. measured from apex, ft
X_o	= location of transition front measured from apex, ft
α	= angle of attack, rad
$\bar\alpha_{RMS}$	= root-mean-square angle of attack, rad
Θ_c	= cone half-angle, deg
$\delta_B{}^*$	= boundary-layer displacement thickness at vehicle base, ft
Φ_α	= power spectrum of angle of attack, (rad)^2/rad/sec
Φ_{12}	= cross spectrum of pressures, (psf)^2/rad/sec
Φ	= power spectrum of pressures, (psf)^2/rad/sec
ω_o	= vehicle pitch frequency, rad/sec

I. Introduction

IT is well known that re-entry vehicles (R/V's) exhibit periods of dynamic instability resulting in angle-of-attack excursions. This is illustrated in Fig. 1 where angle-of-attack divergences and reconvergences are shown for a typical nonablator, a low ablator, and a high ablator. These instabilities are known to occur for sharp and blunt cones, small and large R/V's, low and high W/C_DA vehicles, and R/V's with stable stability derivatives.

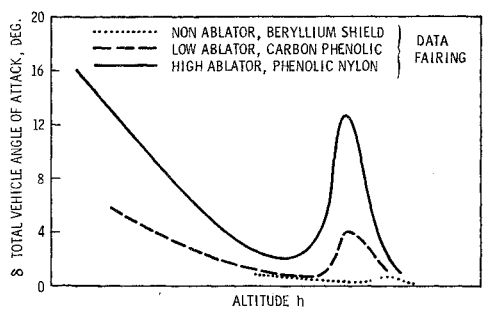

Fig. 1 Angle of attack divergence for various ablating R/V's—maximum envelopes.

As a result of this unstable behavior and its possible detrimental effect on the operational performance parameters, a concentrated effort was undertaken throughout the aerospace industry[1–5] to understand the causative factors producing this instability phenomenon; various hypotheses and theories were proposed during the last decade to provide an explanation. Possible causes and analytical approaches conducted to date to provide an explanation to various instances of the over-all divergence problem are presented as follows: 1) nose breakage, nose and structural resonance; 2) pitching moment hysteresis, vortex shedding and separation at high angle of attack; 3) roll effects, higher order and nonlinear terms in the equations of motion; 4) unstable dynamic damping coefficients ($C_{mq} + C_{m\dot\alpha}$); 5) boundary-layer transition effects ($\dot m$ effects); 6) pressure response lag in boundary layer; and 7) asymmetric transition and nonlinear C_m and C_N due to mass addition.

The majority of these methods are inadequate for flight vehicle instability predictions. While some of these parameters may aggravate or relieve the stability problem, they are not believed to be primary causative factors.[6]

A theory is proposed in this paper which does provide an analytical solution and a plausible mechanism to one type of dynamic stability problem of re-entry vehicles and which should help explain heretofore unexplained motion perturbations at transition.

Presented as Paper 73-180 at AIAA 11th Aerospace Sciences Meeting, January 10–12, 1973, Washington, D.C.; submitted March 7, 1973; revision received July 19, 1973.

Index categories: LV/M Dynamics, Uncontrolled; LV/M Flight Testing; Entry Vehicle Dynamics and Control.

* Consulting Engineer, Aerodynamics Laboratory, Re-Entry and Environmental Systems Division.

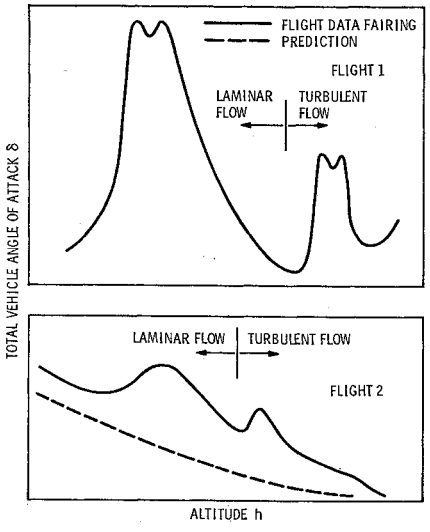

Fig. 2 Total angle of attack histories—maximum envelopes.

II. Method of Approach

It is presently believed that there are two basic and distinct mechanisms producing vehicle dynamic instability. The first has been observed in fully laminar flow and the second during boundary-layer transitional flow as shown in Fig. 2. The proposed solution will be concerned only with the phenomenon in transitional flow.

It was very convenient that some of the highly divergent vehicles did not roll, thereby reducing the unwieldy six degrees-of-freedom equations of motion to an approximate single degree of freedom pitch equation

$$I_{\ddot{\alpha}} = \text{total pitching moment} \tag{1}$$

The fundamental question was posed as to what mechanism could perturb this equation and create an instability. There are two basic types of dynamic instability that could produce the divergent motions observed in flight. The first is a self sustained type of oscillation (flutter) as a result of rigid body mode coupling between aerodynamic and inertial parameters. This type of dynamic instability was eliminated because the aerodynamic coefficients were not considered to vary to such an extent as to produce instability.[6]

The second and most plausible type of dynamic instability is of the forced variety which arises from externally applied loading. Such a loading can be obtained from the random fluctuating pressures that are present in the transitional and turbulent boundary layers. These pressures are essentially nonexistent in laminar flow.[7] This explanation is consistent with vehicle instabilities occurring in the accepted boundary-layer transitional flow regime.[8,9] These pressures begin to affect the motion as soon as the transition front moves onto the vehicle aft surface as shown in Fig. 3. The significant and most important fact is that the pressure fluctuations give rise to a local fluctuating force and therefore moment about the vehicle center of gravity.

Introducing the instantaneous total pitching moment from Fig. 3 including quasi-static aerodynamics into Eq. (1) yields:

$$I\ddot{\alpha} + B_{\dot{\alpha}}\dot{\alpha} + A_{\alpha}\alpha = M(t) \tag{2}$$

where

$$A_{\alpha} = -q_{\infty}S_{\text{REF}}D_{\text{REF}}C_{m\alpha}$$

$$B_{\dot{\alpha}} = -q_{\infty}S_{\text{REF}}\left[C_D - C_{N\alpha} + (C_{mq} + C_{m\dot{\alpha}})\frac{D_{\text{REF}}{}^2M}{2I}\right]\frac{I}{MU_{\infty}}$$

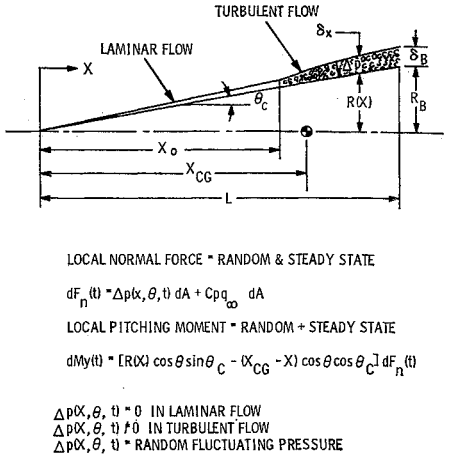

Fig. 3 Method of approach.

The forcing function $M(t)$ in Eq. (2) is actually a randomly applied time dependent moment resulting from the random boundary-layer fluctuating pressures

$$M(t) = \int_0^{2\pi}\int_{X_o}^{L} R(X)\left[X_{CG} - \frac{X}{\cos^2\Theta_c}\right]\Delta\tilde{p}(X,\ \Theta,\ t)\cos\Theta d\Theta dX \tag{3}$$

where the integration is performed from the transition front X_o to the vehicle base L. The time variation of the pressures, $\Delta p(X,\Theta,t)$, are essentially nonexistent in laminar flow ($X_o \geq L$) but will be present as soon as the transition front moves onto the aft surface ($X_o < L$).

For a statically and dynamically stable vehicle, Eq. (2) will become unstable if the forcing function $M(t)$ resonates with the fundamental R/V pitch frequency. The power spectrum of fluctuating pressures in transitional and turbulent flow does contain pressures that are fluctuating at frequencies in tune with the vehicle motion frequency and thus can produce instability. This is analogous to buffeting and ground wind loads generated on launch vehicles. Ground test data in Fig. 4 clearly indicate that the root bending moment (system response) due to ground wind loads (random input due to fluctuating pressures) on axisymmetric launch vehicles is random in magnitude, but in tune with the fundamental system frequency.[10] Vehicle response due to random buffeting loads produces similar results.[11]

Because of the random nature of the problem, the solution of Eq. (2) will be obtained in the frequency domain (as opposed to the conventional time domain) in which only the mean square response can be evaluated utilizing the power spectral density methods of generalized harmonic analysis.[12-14] The conversion of Eq. (2) into spectral terms leads to the following spectral equation for the angle of attack response

$$\Phi_{\alpha} = \frac{Q_{\alpha}{}^2}{I^2\omega_o{}^4}\frac{1}{\{[1-(\omega/\omega_o)^2]^2 + [(B_{\dot{\alpha}}/I\omega_o)(\omega/\omega_o)]^2\}} \tag{4}$$

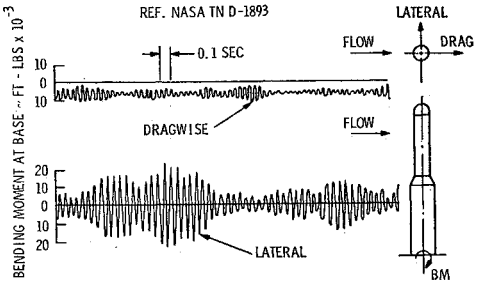

Fig. 4 Ground-wind loads on axisymmetric launch vehicles.

And the mean square angle of attack response is obtained by integrating Eq. (4) over all the frequencies

$$\overline{\alpha^2} = \int_0^\infty \Phi_\alpha d\omega \tag{5}$$

An approximate solution to Eq. (5) has been developed in the appendix and yields

$$\overline{\alpha^2} = \frac{1}{A_\alpha B_{\dot\alpha}}\left[\frac{\delta_B^*}{U_c}(\bar{P}_{\text{RMS}})^2\right]\left[2\pi\frac{\delta_B^*}{C_2 R_B}\right] R_B^2 L^4 f(X_{CG}, X_o, \Theta_c) \tag{6}$$

This is the mean square angle of attack to which the R/V will diverge during transition. The total vehicle angle of attack is then

$$\alpha\Big|_{3\sigma} = \alpha_{\text{MOTION}} + 3(\overline{\alpha^2})^{1/2} \tag{7}$$

A 3σ root-mean-square (RMS) value is utilized which implies that 99.73% of the time the peak oscillating angle of attack, due to fluctuating pressures only, will be less than the 3σ value. It is assumed that the oscillatory angle of attack has a normal distribution. The RMS value of the angle of attack response is then equivalent to the standard deviation (σ) since the mean is zero. It should be noted that by including tolerances on the aerodynamic terms, larger values of the total angle of attack (α_T) could be obtained. The nominal values have been utilized in this analysis.

Equation (7) indicates that an oscillating re-entry vehicle which is stable in laminar flow ($\bar{\alpha}_{\text{RMS}} = 0$) will incur an angle-of-attack divergence in transitional and turbulent flow whose magnitude is directly dependent on the various parameters shown in Eq. (6). The validity of the proposed dynamic stability theory as a technique for predicting R/V instability during boundary-layer transition will be discussed below.

III. Discussion of Results

An inspection of Eq. (6) reveals that the mean square angle-of-attack divergence is a function of many variables such as: fluctuating pressure level, configuration and size, heat shield material, transition progression, and static and dynamic stability coefficients (steady pressure). These effects and others not immediately apparent will be discussed with respect to flight observed instabilities.

Effect of Dynamic Pressure

Flight data of many highly divergent R/V's have indicated that divergence and reconvergence can occur prior to peak dynamic pressure. It was concluded that the effect of dynamic pressure should not be a first-order contribution to vehicle dynamic instabilities. The proposed theory as well should be independent of dynamic pressure. For instance, the root-mean-square (RMS) fluctuating pressure $\bar{p}_{\text{RMS}} \approx q_\infty$ and $A_\alpha \approx q_\infty$ while $B_{\dot\alpha} \approx q_\infty/U_\infty$, which upon substitution into Eq. (6), will make the mean square angle-of-attack response independent of both the dynamic pressure q_∞ and the free-stream velocity U_∞ since $U_c \approx U_\infty$.

Effects of Static and Dynamic Stability Coefficients

It is noted from Eq. (6) that the magnitude of the angle-of-attack divergence is inversely proportional to both the static and dynamic stability coefficients. Thus, an increase in $C_{m\alpha}$ will decrease $\overline{\alpha^2}$ while a decrease in $C_{m\alpha}$ will increase the magnitude of $\overline{\alpha^2}$. The same is true for the dynamic stability coefficient ($C_{mq} + C_{m\dot\alpha}$). Preflight prediction of these coefficients should include estimates of the effects of mass addition, nose bluntness, and possibly asymmetric transition since these could influence their magnitudes.

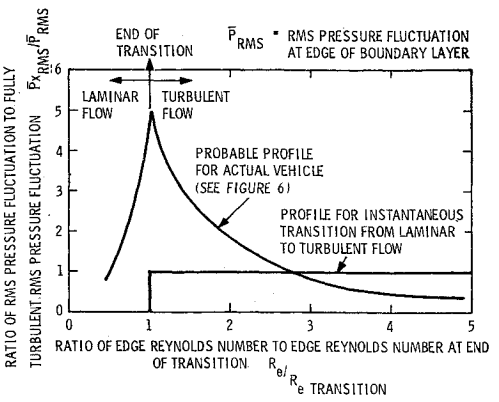

Fig. 5 Root-mean-square pressure fluctuation profiles.

Fluctuation Pressure Levels

The RMS fluctuating pressure $\bar{p}_{\text{RMS}}$ is one of the more critical parameters influencing the magnitude of $\overline{\alpha^2}$ in Eq. (6). It is also the most difficult one to predict because of the limited acoustic pressure data available at hypersonic speeds. Theoretical predictions have been developed[1-5] for smooth nonablating surfaces in fully turbulent flow. This would assume that the transition profile from laminar to turbulent flow occurs instantaneously as a step function as indicated in Fig. 5. In this same figure is also shown the transition front as it may occur on an actual vehicle. This curve is based on the RMS pressure fluctuations profiles of Fig. 6 obtained with a flush mounted surface microphone on a smooth nonablating sharp $\Theta_c = 5°$ model.[7] Other areas in which there are little or no data available for evaluation are the effects of mass addition and roughness on these fluctuating pressures.

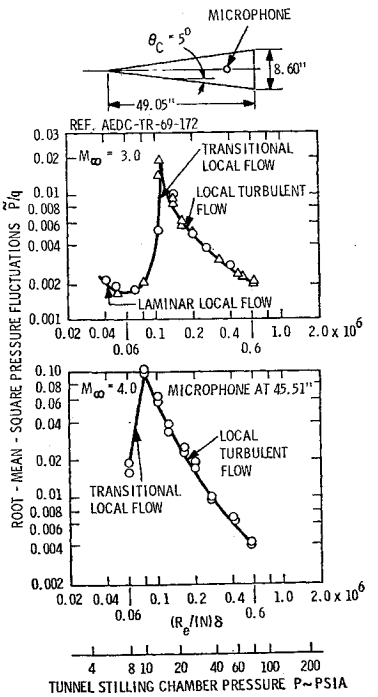

Fig. 6 RMS Pressure fluctuation profiles.

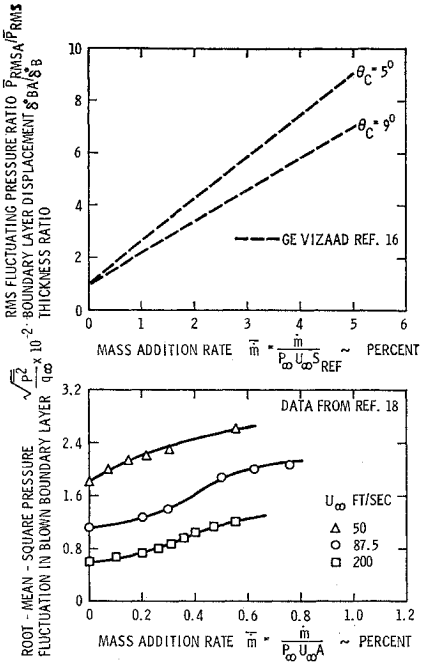

Fig. 7 Effects of mass addition on boundary layer displacement thickness and RMS fluctuation pressure.

Effects of Mass Addition on δ_B^* and $\bar{p}_{RMS}$

The boundary-layer displacement thickness δ_B^* is another critical parameter influencing the magnitude of $\overline{\alpha^2}$ in Eq. (6). The effect of mass addition is known to increase the boundary layer displacement thickness δ_B^* on the vehicle surface. Theoretical calculations[16] produced the results in Fig. 7 which show a nearly linear variation with the integrated mass addition rate $\dot{m}$ in fully turbulent flow. These curves should be upgraded with available test data.[17] For the present illustration, the analytical results in Fig. 7 are considered adequate.

There are no fluctuating pressure data known that includes mass addition with the exception perhaps of results obtained in subsonic flow[18] and presented in Fig. 7. It appears that mass addition to the boundary-layer increases the RMS pressures $\bar{p}_{RMS}$ which would again increase $\overline{\alpha^2}$. For simplicity and until data become available with respect to mass addition and also roughness in hypersonic flow, it is assumed that $\bar{p}_{RMS}$ varies identically as δ_B^* as shown in Fig. 7.

Transition Front Progression

The validity of the present proposed theory given by Eq. (6) is now tested by requiring that flight vehicles enter the divergence region as well as exit for a transition front progressing from the vehicle base to its nose. This is accomplished through the function $f(X_{CG}, X_o, \Theta_c)$ in Eq. (6). This function has been crudely evaluated in the Appendix to illustrate its behavior with transition front movement. Figure 8 presents results for two sharp cone vehicles with semiapex cone angles of $\Theta_c = 5°$ and 10° and typical c.g. These results were obtained by numerically integrating Eq. (A15) in the Appendix with $C_1 = 0$. It should be noted that the magnitude and shape of this function will be affected by both the pressure fluctuation and boundary-layer displacement thickness profiles presented in Fig. 5 and given by Eq. (A10), respectively. For illustrative purposes, however, the results in Fig. 8 are adequate.

The behavior of $f(X_{CG}, X_o, \Theta_c)$ when introduced into Eq. (6) demonstrates that while the transition front is off the vehicle base ($X_o \geq L$), the function $f(X_{CG}, L, \Theta_o) = 0$, and

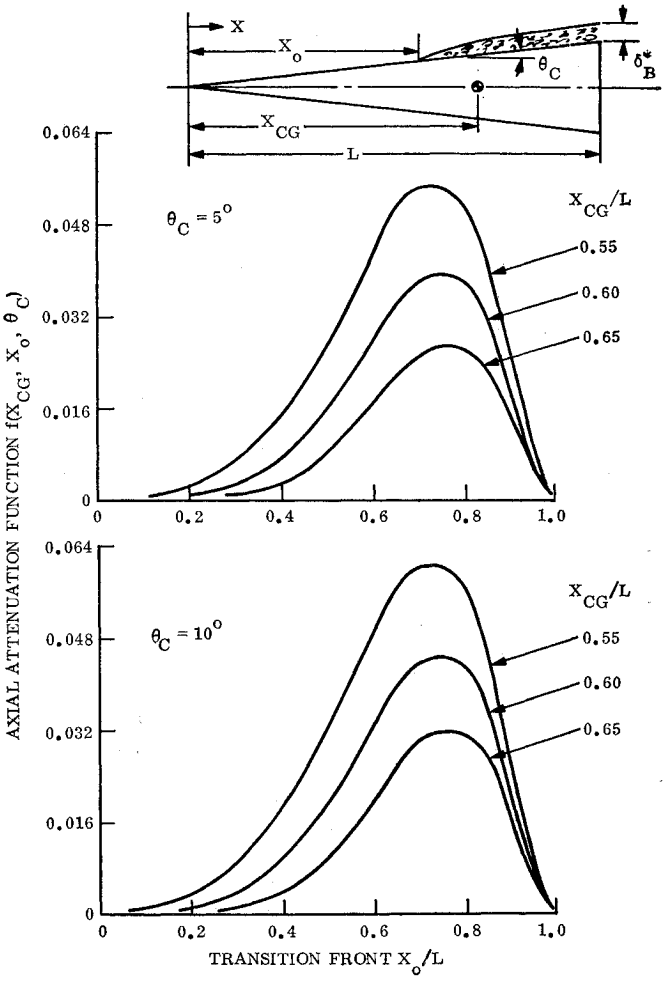

Fig. 8 Axial attenuation function $f(X_{cg}, X_o, \Theta_c)$

there is no angle-of-attack divergence. The RMS pressure $\bar{p}_{RMS} = 0$ as well, in laminar flow. When the transition front moves onto the vehicle aft surface ($X_o < L$, $\bar{p}_{RMS} \neq 0$), an angle-of-attack divergence will ensue which increases in amplitude following the trend of $f(X_{CG}, X_o, \Theta_c)$. This is followed by a decrease in amplitude (according to Fig. 8) as the transition front progresses past the c.g. until it reaches the nose where it will have negligible influence on the magnitude of $\overline{\alpha^2}$. The function $f(X_{CG}, X_o, \Theta_c) = 0$ while $\bar{p}_{RMS} \neq 0$ when the transition front reaches the vehicle nose. Thus, both entry and exit of the vehicle into the divergence region are now accounted for.

For a specific vehicle, the time required for transition to move from the vehicle base to the nose is of great importance since it will influence the maximum angle of attack to which the vehicle will diverge. For instance, if the transition front traverses the vehicle rapidly, there should be insufficient time for the vehicle angle of attack to build up to its maximum potential value, as determined by Eq. (6). If, on the other hand, the transition front traverses the vehicle slowly, then there will be ample time for the angle of attack to build up to its maximum amplitude. Equation (6) is valid only for the latter case and cannot account for a time dependent transition front movement.

IV. Correlation with Flight Data

Calculations were conducted on the same R/V's shown in Fig. 1 applying Eqs. (6) and (7). The resulting angle-of-attack histories are presented for the nonablating beryllium heat shield in Fig. 9, for the low ablating carbon phenolic

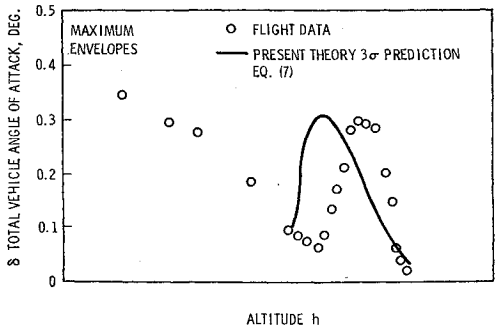

Fig. 9 Angle of attack divergence for nonablator beryllium heat shield.

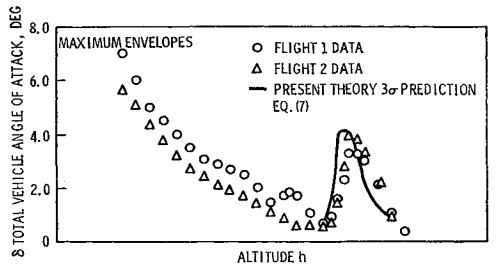

Fig. 10 Angle of attack divergence for low ablator carbon phenolic heat shield.

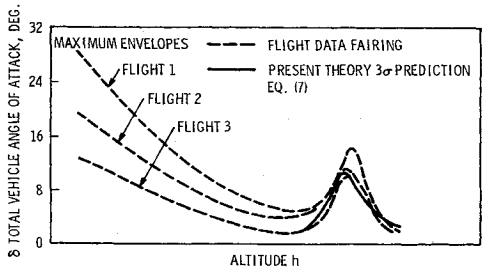

Fig. 11 Angle of attack divergence for high ablator phenolic nylon heat shield.

heat shield in Fig. 10, and for the high ablating phenolic nylon heat shield in Fig. 11. It is observed that correlation of the present theory using Eqs. (6) and (7) with flight data is generally excellent in trend but appears to be slightly low in magnitude.

There can be large tolerances associated in the preflight prediction of parameters such as δ_B^*, RMS pressures $\bar{p}_{\text{RMS}}$ which require local flow properties at the boundary-layer edge. There are also uncertainties associated with nose shape changes, bluntness ratio, mass addition, and the effect of asymmetric transition which is known to have a large influence on the RMS pressures $\bar{p}_{\text{RMS}}$.

The preceding point out that both ground and flight tests are required to verify the many parameters affecting the angle-of-attack divergence given by Eq. (6).

V. Conclusions

The proposed theory is believed to provide a basic and more general contribution to the solution to the dynamic instability problem of R/V's during transition because: 1) the present fluctuating pressure mechanism accounts for the R/V exit as well as the entry into the angle-of-attack instability region; 2) preflight angle-of-attack perturbations due to pressure fluctuations can be calculated without recourse to the more grossly empirical $(C_{mq} + C_{m\dot{\alpha}})$ stability coefficients; 3) the present theory appears to correlate with both high and low ablators and other data indicates that it is also applicable to both large and small R/V's.

Appendix

The simplified pitch equation of motion including the effects of fluctuating pressures acting on the vehicle surface in transitional and turbulent flow Fig. 3 is

$$I\ddot{\alpha} + B_{\dot{\alpha}}\dot{\alpha} + A_{\alpha}\alpha = \int_{X_0}^{L}\int_{0}^{2\pi} dM(t) \tag{A1}$$

The spectral equation for the angle-of-attack response utilizing the power spectral density methods of Ref. 16 for instance is

$$\Phi_{\alpha} = \frac{Q_{\alpha}{}^2}{I^2\omega_o{}^4}\frac{1}{\{[1-(\omega/\omega_o)^2]^2 + [(B_{\alpha}/I\omega_o)(\omega/\omega_o)]^2\}} \tag{A2}$$

which yields the mean square angle of attack after integration over all the frequencies

$$\overline{\alpha^2} = \int_0^{\infty} \Phi_{\alpha} d\omega \tag{A3}$$

Thus, it is only necessary to evaluate the function $Q_{\alpha}{}^2$ given by

$$Q_{\alpha}{}^2 = \int_{X_0}^{L}\int_{X_0}^{L}\int_0^{2\pi}\int_0^{2\pi} \Phi_{12}\cos^2\Theta_c \cos\Theta_2 \cos\Theta_1 f(X_2)f(X_1)dA_2dA_1 \tag{A4}$$

where

$$f(X_2) = \left(X_{CG} - \frac{X_2}{\cos^2\Theta_c}\right); \qquad (fX_1) = \left(X_{CG} - \frac{X_1}{\cos^2\Theta_c}\right)$$

$$dA_2 = \frac{R(X_2)dX_2d\Theta_2}{\cos\Theta_c}; \qquad dA_1 = \frac{R(X_1)dX_1d\Theta_1}{\cos\Theta_c}$$

$$\Phi_{12} = \Phi(\omega,X)e^{-C_1|X_2-X_1/\delta X^*|}e^{-C_2|Y_2-Y_1/X^*|}\cos\frac{\omega(X_2-X_1)}{U_c} \tag{A5}$$

Equation (A5) is the cross-spectrum of pressures at two different points (X_2, Y_2) and (X_1, Y_1) on the surface.

$$\Phi(\omega,X) = \frac{2}{\pi}\frac{\delta_X^*}{U_c}(\bar{p}_{\text{RMS}})^2\frac{1}{1+(\omega\delta_X^*/U_c)^2} \tag{A6}$$

Equation (A6) is the power spectrum of pressures at a given point on the surface. Since the convection velocity U_c is very large in hypersonic flow and only freuqencies ω in the order of the vehicle pitch frequency ω_o are of concern, the term $\cos[\omega(X_2 - X_1)/U_c] = 1$ and $\omega\delta_X^*/U_c = 0$. The power spectrum of pressures $\Phi(\omega,X)$ may be considered as the product of two functions, namely

$$\Phi(\omega,X) = \Phi(\omega)\Phi(X) \tag{A7}$$

where

$$\Phi(\omega) = (2/\pi)(\delta_B^*/U_c)(\bar{p}_{\text{RMS}})^2 \tag{A8}$$

$$\Phi(X) = (\delta_X^*/\delta_B^*)[(\bar{p}_{X_{\text{RMS}}})^2/(\bar{p}_{\text{RMS}})^2] \tag{A9}$$

Both the boundary-layer displacement thickness δ_X^* and the RMS fluctuation pressure $\bar{p}_{X_{RMS}}$ are functions of the axial distance (see Fig. 5).

Estimates of the boundary-layer displacement thickness in turbulent flow have shown the following functional relationship with axial distance[16]:

$$\delta_X^*/\delta_B^* = [(\eta - \eta_o)/(1 - \eta_o)]^{0.8(1-\eta_o)} \quad \text{(A10)}$$

where

$$\eta = X/L \quad \text{and} \quad \eta_o = X_o/L$$

The cross-spectrum of pressures given by Eq. (A5) taking into account the axial variations is now

$$\Phi_{12} = \Phi(\omega)[\Phi(X_2)\Phi(X_1)]^{1/2} e^{-C_1|X_2 - X_1/\delta X^*|\Theta_2 - \Theta_1|} e^{-C_2 R(X)/\delta X^*|\Theta_2 - \Theta_1|} \quad \text{(A11)}$$

where for conical bodies $Y_2 = R(X)\Theta_2$ and $Y_1 = R(X)\Theta_1$.

The coefficients C_1 and C_2 are determined by empirically fitting the cross-correlation function with data. Values of $C_1 = 0.05$ and $C_2 = 0.6$–1.0 yield good data matching.

It has been assumed up to this point in the development that the transition front is symmetrical. While the solution to the problem is affected by asymmetric transition due to angle of attack for instance, the added complexity resulting from asymmetric transition is not justified at this time. It is nonetheless recognized that inclusion of this effect may be not only desirable but required for accurate quantitative predictions.

Substituting Eq. (A11) into Eq. (A4) and integrating circumferentially by carefully taking into account the absolute sign shown in the exponential function yields for turbulent boundary-layer pressure fluctuations in which $R(X)/\delta_X^* \gg 1$

$$Q_\alpha{}^2 = \Phi(\omega) \int_{X_o}^{L} \int_{X_o}^{L} [\Phi(X_2)\Phi(X_1)]^{1/2} e^{-C_1|X_2 - X_1/\delta X^*|} \times f(X_2) f(X_1)\, g(X_2, X_1) R(X_2) R(X_1) dX_2 dX_1 \quad \text{(A12)}$$

The function $g(X)$ was determined from

$$g(X) = \int_0^{2\pi} \int_0^{2\pi} e^{-C_2 R(X)/\delta X^*|\Theta_2 - \Theta_1|} \cos\Theta_2 \cos\Theta_1 d\Theta_2 d\Theta_1 \quad \text{(A13)}$$

which for $R(X)/\delta_X^* \gg 1$ simplifies to

$$g(X_2, X_1) \cong \frac{2\pi}{C_2} \left[\frac{\delta_{X2}^* \delta_{X1}^*}{R(X_2)R(X_1)}\right]^{1/2} \quad \text{(A14)}$$

Substituting Eq. (A14) into Eq. (A12) and nondimensionalizing with $R(X) = \eta R_B$ and $dX = Ld\eta$ there results

$$Q_\alpha{}^2 = 2\pi\Phi(\omega)\left(\frac{\delta_B^*}{C_2 R_B}\right) R_B{}^2 L^4 \int_{\eta_o}^{1}\int_{\eta_o}^{1} \left(\frac{\eta_2 - \eta_o}{1 - \eta_o}\right)^{0.8(1-\eta_o)} \left(\frac{\eta_1 - \eta_o}{1 - \eta_o}\right)^{0.8(1-\eta_o)} \left(\frac{\bar{p}_{\eta 2 RMS}}{\bar{p}_{RMS}}\right)\left(\frac{\bar{p}_{\eta 1 RMS}}{\bar{p}_{RMS}}\right) \times e^{-C_1 L|\eta_2/\delta\eta 2^* - \eta_1/\delta\eta 1^*|} f(\eta_2) f(\eta_1)(\eta_2\eta_1)^{1/2} d\eta_2 d\eta_1 \quad \text{(A15)}$$

As observed in Fig. 5, the RMS fluctuating pressure ratio $\bar{p}_{\eta 2 RMS}$ is a function of the axial distance considering the fact that the Reynolds number varies with axial distance along the body surface.

Integration of Eq. (A15) is performed numerically from the transition front to the vehicle aft end. It should be noted that turbulent flow is assumed to begin at η_o according to Eq. (A10) and that no moment contributions arise when $\eta \leqslant \eta_o$ as shown in Fig. A1.

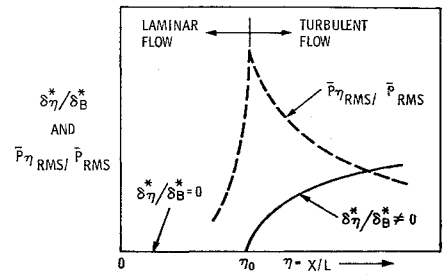

Fig. A1 Axial variation of RMS pressure and boundary-layer thickness ratios.

For simplification Eq. (A15) is defined as

$$Q_\alpha{}^2 = 2\pi\Phi(\omega)(\delta_B^*/C_2 R_B) R_B{}^2 L^4 f(X_{CG}, X_o, \Theta_c) \quad \text{(A16)}$$

where the function $f(X_{CG}, X_o, \Theta_c)$ is obtained by integration of Eq. (A15). Since $f(X_{CG}, X_o, \Theta_c)$ is independent of the frequency, the mean square angle of attack can be determined from Eq. (A3) utilizing Eqs. (A16) and (A2). The resulting mean square angle of attack is

$$\overline{\alpha^2} = \frac{2\pi}{A_\alpha B_{\dot\alpha}} \left(\frac{\delta_B^*}{C_2 R_B}\right)\left[\frac{\delta_B^*}{U_c}(\bar{p}_{RMS})^2\right] R_B{}^2 L^4 f(X_{CG}, X_o, \Theta_c) \quad \text{(A17)}$$

The preceding results were obtained from the following integrations performed on Eq. (A2)

$$\int_0^\infty \frac{\Phi(\omega)d\omega}{I^2\omega_o{}^4\left\{\left[1 - \left(\frac{\omega}{\omega_o}\right)^2\right]^2 + \left[\frac{B_\alpha}{I\omega_o}\left(\frac{\omega}{\omega_o}\right)\right]^2\right\}} \cong \frac{\pi}{2}\frac{\Phi(\omega_o)}{A_\infty B_{\dot\alpha}} \quad \text{(A18)}$$

which upon substituting Eq. (A8) yields the term given by the bracket in Eq. (A17).

References

[1] *Transactions of the Second Technical Workshop on Dynamic Stability Testing*, Vols. I–III, Arnold Engineering Development Center, Arnold Air Force Station, Tenn., April 20–22, 1965.

[2] *Transactions of the Third Technical Workshop on Dynamic Stability Problems*, Vols. I–VI, NASA Ames Research Center, Moffett Field, Calif., Nov. 4–7, 1968.

[3] Waterfall, A. P., "Effect of Ablation on the Dynamics of Spinning Re-Entry Vehicles," *Journal of Spacecraft and Rockets*, Vol. 6., No. 9, Sept. 1969, pp. 1038–1044.

[4] Ibrahim, S. K., "Effects of Ablation on the Pitching Moment Derivatives of Cones in Hypersonic Flow," Rept. 0414-4, April, 1967, Fluidyne Engineering Corp., Minneapolis, Minn.

[5] Martellucci, A. and Neff, R. S., "The Influence of Asymmetric Transition on Re-Entry Vehicle Motion," *Journal of Spacecraft and Rockets*, Vol. 8, No. 5, May 1971, pp. 476–482.

[6] Kirsch, A. A., "A Proposed Dynamic Stability Solution," ALDM 72-115, March, 1972, GE Aerodynamics Laboratory Data Memo, Philadelphia, Pa.

[7] Pate, S. R., "Measurements and Correlations of Transition Reynolds Number on Sharp Slender Cones at High Speeds," AEDC TR-69-172, Dec. 1969, Von Karman Gas Dynamics Facility, Arnold Engineering Development Center, Arnold Air Force Base, Tenn.

[8] Sacks, I. and Schurmann, E. E. H., "Aerodynamic Phenomena Associated with Advanced Re-Entry Systems," RAD-TM63-79, Dec. 1963, AVCO Corp., Wilmington, Mass.

[9] Crusciel, G. T. and Chang, S. S., "Effects of Ablation on Hypersonic Aerodynamic Stability Characteristics," AIAA Paper 66-410, Los Angeles, Calif., 1966.

[10] Buell, D. A., McCullough, G. B., and Steinmetz, W. J., "A Wind-Tunnel Investigation of Gound-Wind Loads on Axisymmetric Launch Vehicles," TN D-1893, Oct. 1963, NASA.

[11] Andrews, J. S., "The Effects of Transonic Buffeting on a Hammerhead Shaped Payload," *AIAA Symposium on Structural Dynamics and Aeroelasticity*, Boston, Mass., Aug. 30–Sept. 1, 1965.

[12] Bisplinghoff, R. L., Ashley, H., and Halfman, R. L., *Aeroelasticity*, Addison-Wesley Publishing Co., Reading, Mass., 1965

[13] Goldberg, A. P. and Wood, J. D., "Dynamic Loads on the Atlas Able 5 During Transonic and Low Supersonic Speeds," STL/TM 60-0000-19075, Aug. 22, 1960, Space Technology Laboratories, Los Angeles, Calif.

[14] Houbolt, J. C., "Structural Response of Re-Entry Vehicles to Boundary Layer Noise," GE-RESD, TIS 65SD223, March, 1965, General Electric, Philadelphia, Pa.

[15] Houbolt, J. C., "On the Estimation of Pressure Fluctuations in Boundary Layers and Wakes," GE-RESD, TIS 66SD296, Aug., 1966, General Electric, Philadelphia, Pa.

[16] Studerus, C. J. and Dienna, E. A., "Viscous Interaction Zero Angle of Attack Drag (VIZAAD) Program," GE, TIS 64SD292, Nov. 1964, General Electric, Philadelphia, Pa.

[17] Martellucci, A. and Rie, H., "Effects of Mass Addition on Viscous Flow Parameters," SAMSO TR-71-60, also GE TIS 71SD205, March, 1971, General Electric, Philadelphia, Pa.

[18] Rosenbaum, H. and Margolis, D. P., "Pressure Fluctuations Beneath an Incompressible Turbulent Boundary Layer with Mass Addition," *The Physics of Fluids*, Vol. 10, No. 6, June 1967.

DECEMBER 1973 J. SPACECRAFT VOL. 10, NO. 12

Application of Sequential Filtering to Estimation of the Interplanetary Orbit of Mariner 9

KENNETH H. ROURKE* AND JAMES F. JORDAN†
Jet Propulsion Laboratory, Pasadena, Calif.

This paper presents the results of the application of sequential filtering to the determination of the interplanetary orbit of the Mariner 9 spacecraft. The technique is a specific extension of the Kalman filter. The special problems associated with applying this technique are discussed and the particular algorithmic implementations are outlined. The method is compared against the weighted least squares filters of conventional application. The results reveal that relatively simple sequential filter configurations yield solutions superior to those of the conventional method when applied to radio measurements of Mariner 9.

Nomenclature

X = spacecraft position vector
V = spacecraft velocity vector
u = spacecraft nongravitational accelerations
Z = $F(X, V, t)$, observational data vector
ε = observation error
x = $[(X - X_{\text{nominal}})^T, (V - V_{\text{nominal}})^T]^T$ position and velocity, i.e., "state" deviation vector
z = $Z - Z_{\text{nominal}}$, observational data deviation vector
$(\cdot)^T$ = transpose operation
T_k = filter batch break times
x_k = $x(T_k)$, discretized state
$\Phi(T_{k+1}, T_k)$ = $\partial x_{k+1}/\partial x_k$, state transition matrix
$\Gamma(T_{k+1}, T_k)$ = $\partial x_{k+1}/\partial u_k$, acceleration transition matrix
z_k = $[z^T(t_1), \ldots, z(t_{n_k})]^T$, $T_k \leq t_1, \ldots, t_{n_k} \leq T_{k+1}$, data vector for data in batch $[T_k, T_{k+1}]$
A_k = $\partial z_k/\partial x_k$, state data partial derivatives
B_k = $\partial z_k/\partial u_k$, acceleration data partial derivatives
Δv = velocity increment vector
$B \cdot T$ = component of spacecraft asymptotic miss vector in the ecliptic plane
$B \cdot R$ = component of spacecraft asymptotic miss vector normal to the ecliptic plane
Δa = spacecraft acceleration correction model

Presented as Paper 72-906 at the AIAA/AAS Astrodynamics Conference, Palo Alto, Calif., September 11–12, 1972; submitted October 30, 1972; revision received July 27, 1973. This paper presents one phase of research carried out at the Jet Propulsion Laboratory, California Institute of Technology, under NASA Contract NAS7-100.

Index categories: Spacecraft Navigation, Guidance, and Flight-Path Control Systems; Spacecraft Tracking; Navigation, Control, and Guidance Theory.

* Senior Research Engineer, Interplanetary Orbit Determination Group.

† Group Supervisor, Satellite Orbit Determination and Planetology Group.

Introduction

OVER the past decade the navigation of the United States' interplanetary spacecraft has relied almost exclusively on Earth based radio orbit determination. Radio orbit determination accuracies have improved by more than an order of magnitude during the last 10 years; from the errors of 1300 km encountered during the Mariner 2 mission to Venus in 1962, to the 50-km errors experienced in navigating Mariner 9 to Mars in 1971.

These performance improvements have been brought about by the concurrent improvements made in the quality of the basic radio orbit determination data types, range and range rate, now accurate to 15m and 1 mm/sec, respectively.

The remaining errors which affect the accuracy of interplanetary orbit determination are uncertainties in the measurement and spacecraft dynamics models which produce range change errors when matching passes of tracking data to estimated orbits.

A major error arises from the diurnal range change due to uncertainties in the tracking stations' Earth-fixed coordinates. Indeed, uncertainties in the locations of the tracking stations are the principal limitation to determination of spacecraft geocentric angles from single passes of tracking data. Current station location errors of 3–7 m, which include the equivalent effects of both charged and neutral particles on the radio signal, can produce orbit estimate errors of approximately 100–200 km at typical Earth-Mars encounter distances.[1]